

# Enhancing Minefield Detection: A Robotic Approach for Multisensor Detection and Discrimination of Small Low-Metal-Content Landmines

Lorenzo Capineri<sup>ID</sup>, Senior Member, IEEE, Gennadiy P. Pochanin<sup>ID</sup>, Senior Member, IEEE, Vadym P. Ruban<sup>ID</sup>, Luca Bossi, Pierluigi Falorni<sup>ID</sup>, Tetiana Ogurtsova, Timothy D. Bechtel<sup>ID</sup>, Member, IEEE, and Fronefield Crawford<sup>ID</sup>

**Abstract**—We provide experimental results of an investigation into the detectability of small, low-metal-content (LMC) landmines using multiple sensors in field conditions. The sensors tested were an impulse ground penetrating radar (GPR), a metal detector (MD), and a holographic subsurface radar (HSR). By using the combined sensors, we were able to reliably detect the presence of both M14 and Type 72 landmines buried at shallow depths in damp soil. The sensors were mounted on a remotely operated robotic platform, which provides enhanced safety in real minefield conditions. The results indicate that this combination of sensors could provide an effective method for safely identifying the presence of minimum metal landmines in real postconflict zones. Such mines are not currently detectable with unmanned aerial vehicles (UAVs), so this ground-based approach is complementary.

**Index Terms**—Holographic subsurface radar (HSR), low-metal-content (LMC) landmines, metal detector (MD), multisensor robotic platform, remote detection, ultrawideband (UWB) impulse ground penetrating radar (GPR).

## I. INTRODUCTION

THE problem of landmine and unexploded ordnance contamination in former and current conflict zones poses a major problem for civilian populations. The latest estimates [1] show that in 2023, more than 5757 people were killed or maimed by landmines; among them 84% were civilians, and 37% were children. Almost three decades after the adoption of the Antipersonnel Mine Ban Treaty, about 60 million people in over 58 countries and territories still live with the risk of landmines on a daily basis. Identifying and removing mines on a large scale is difficult owing to the hazards presented by the mines as well as the difficulty in properly discriminating dangerous mines from ubiquitous conflict zone clutter, which can have similar physical characteristics (e.g., shrapnel, shell casings, food tins, etc.).

Received 21 June 2025; revised 20 September 2025; accepted 7 October 2025. Date of publication 9 October 2025; date of current version 31 October 2025. This work was supported in by NATO SPS Programme Project under Grant G-7563. (Corresponding author: Lorenzo Capineri.)

Lorenzo Capineri, Luca Bossi, and Pierluigi Falorni are with the Department of Information Engineering, University of Florence, 50139 Florence, Italy (e-mail: lorenzo.capineri@unifi.it; capineri@ieee.org).

Gennadiy P. Pochanin, Vadym P. Ruban, and Tetiana Ogurtsova are with the O.Ya. Usikov Institute for Radiophysics and Electronics of the National Academy of Sciences of Ukraine, 61085 Kharkiv, Ukraine (e-mail: gpp@ire.kharkov.ua).

Timothy D. Bechtel and Fronefield Crawford are with the Franklin and Marshall College, Lancaster, PA 17603 USA (e-mail: tbechtel@fandm.edu).

Digital Object Identifier 10.1109/TGRS.2025.3619806

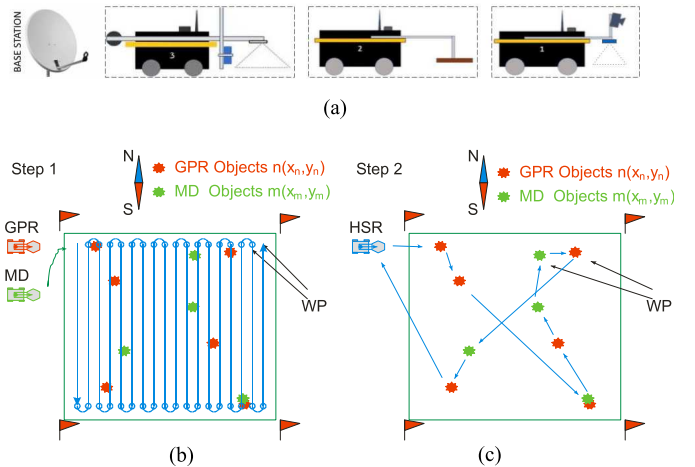


Fig. 1. Landmine detection with three robots. (a) Robots are labeled: 1) for the impulse GPR; 2) for the MD; and 3) for the HSR. (b) Step 1—investigation of the area with GPR and MD robots. (c) Step 2—trajectory of movement of the robot with HSR.

In addition to buried explosives, minefields can contain surface threats. Tripwires can be placed to trigger explosive devices that are intended to deter deminers and demining equipment. Surface (scatterable) mines may also be present. Efforts using optical instruments and LiDAR are underway to efficiently and accurately address these hazards [2], [3].

In this article, we describe a team of cooperating robots equipped with independent complementary sensors. These robots were deployed in a mock minefield to obtain datasets for selected realistic low-metal-content (LMC) mine simulants and common clutter. The detection of these low targets is sometimes difficult even for military grade metal detectors (MDs) in some soil conditions, and here we propose to detect and image these targets with two different ground penetrating radars (GPRs): in accordance with the definition in [4] and [5], we use the term ultrawideband (UWB) Impulse Radar for the time domain type used for the detection and the term holographic subsurface radar (HSR) operating at single frequency in the space domain. The main reason for using HSR is the generation of a microwave hologram of the subsurface object that can be interpreted by a human operator or adequate software [6] for the decision about the nature of the object (man-made or natural). Finally, the HSR at 2 GHz has high

lateral (in-plane) spatial resolution equal to a quarter of the wavelength [7], [8].

The ground-based sensor system described here has some advantages over unmanned aerial vehicle (UAV) or drone investigations, about which there have been numerous recent studies. These include drone experiments using GPRs and synthetic aperture radars (SARs) [9], [10], [11], [12], [13] with autonomous drone navigation [14]. The advantages of a ground-based system over aerial drones include the ability to get very close to the ground (so that the distance to the mine is on the order of centimeters instead of meters), a lack of jitter in the spatial positioning of the sensor if the ground-based sensor platform is still, longer battery life, and the ability of ground robots to maneuver within areas where drones might get tangled in trees or other overhead obstacles (see, e.g., [15] for an overview). These advantages play a major role in detecting LMC antipersonnel (AP) landmines.

## II. MISSION STRATEGY WITH THREE COOPERATING ROBOTS

For this work, we use a common shared robotic platform, the Clearpath Jackal [16]. Robot 1 (shown on the right in Fig. 1) carries an optical camera for detection of tripwires and surface threats and performs the first subsurface investigation using a one-transmitter, four-receiver (1TX-4 RX) UWB or impulse GPR. This system is capable of rapidly performing an initial detection and localization of buried objects (including nonmetal targets) from the differential time-of-flight (TOF) measured at each receiver. This robot also detects surface objects with an optical camera [2]. The camera images are fed to an AI algorithm trained to detect tripwires and specific surface threats such as scatterable mines. Robot 2 (shown in the center of Fig. 1) carries a sensitive MD with a relatively wide search lane (even without sweeping, which for simplicity is not performed). Robot 3 (shown on the left in Fig. 1) interrogates targets detected by the GPR or MD using an HSR that is calibrated/corrected for ground surface relief using on-board terrestrial LiDAR. It moves only to where previous robots have identified potential explosive devices and uses an HSR antenna mounted on an electromechanical scanner to create a holographic image in which the size, shape, and surface relief of buried objects can be recognized.

Currently, all robots are equipped with a two-antenna sub-centimeter global navigation satellite system (GNSS). This system can provide both the position and orientation of the robotic cart. The position and sensor data are shared remotely with an operator and with each other. Eventually, the robots and sensor packages will be made interchangeable using a modular mechatronic interface (MMI).

### A. Mission Strategy

We mark the area to be investigated in both the field and in the software (using 4 flags, for example, as shown in the figures). We put all waypoints (WPs; blue circles in Fig. 1) down to provide the trajectory that covers the defined area.

*Step 1:* The GPR moves along the blue line. During movement, the GPR detects objects (represented by red stars), which we denote according to  $n = 1, \dots, N$  objects with coordinates  $(x_n, y_n)$ . These coordinates are sent to the Cloud Unit.

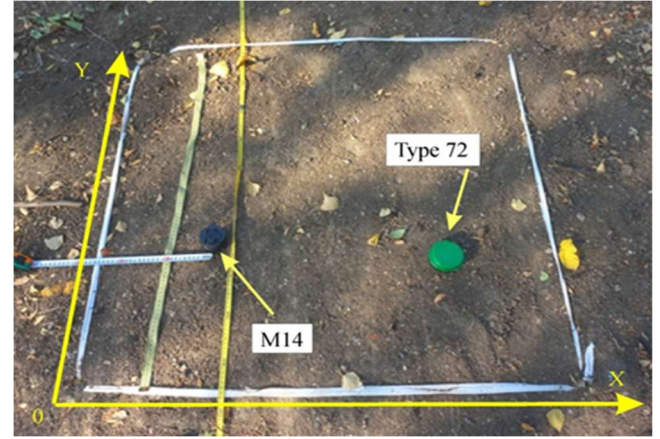


Fig. 2. Designed test field measuring 1 m by 1 m, with the locations of M14 ( $x = 25$  cm,  $y = 30$  cm) and Type 72 ( $x = 75$  cm,  $y = 30$  cm) LMC landmine simulants shown.

We then send the robot with MD along the same trajectory as the GPR. During movement, the MD detects objects (represented by green stars), denoted according to  $m = 1, \dots, M$  objects with coordinates  $(x_m, y_m)$ . These coordinates are sent to the Central Unit. After the MD mission, there are two sets of coordinates: one from the GPR and the other from the MD.

*Step 2:* All of these detected positions become WPs for the HSR. The HSR investigates only these positions identified by the WPs. We can choose an optimal trajectory to spend less time on movement between WPs.

In our system, the decision on what kind of object is detected (such as a mine or inert object, or a false alarm) is done by the HSR. If we detect a suspicious object with impulse GPR and/or MD after scanning it with an HSR, we can conclude that it is either mine or clutter. Only after this decision is made can we estimate such parameters of the ROC curve as True positive, False positive, True negative, or False negative. Only the Impulse GPR and MD mark a location with a suspicious object.

The aim of this article is to demonstrate that remote detection of LMC AP landmines can be performed by using all information collected by the three main sensors installed on the three robots. The detection with handheld MDs follows the standard operative procedure (SOP), but the LMC landmines require them to operate with a small coil distance from the surface and with a high sensitivity setting. In Section III, we describe the field design where M14 and Type 72 LMC AP landmines have been buried for the purposes of this work. In Section IV, we provide a description of the characteristics and operating conditions of the multiple-sensor system. The test field and experiments were replicated by the teams operating in three different countries. In Section V, the real-time detection and positioning results are reported, and a quantitative analysis is presented. Finally, conclusions about the effectiveness of this approach for real field operations are reported.

## III. TEST FIELD DESCRIPTION AND DESIGN

Test fields with the geometry shown in Fig. 2 were constructed in Kharkiv, Ukraine (for testing the GPR), Lancaster, Pennsylvania, USA (for testing the MD), and Florence, Italy (for testing the HSR). The soils at these sites are not identical,

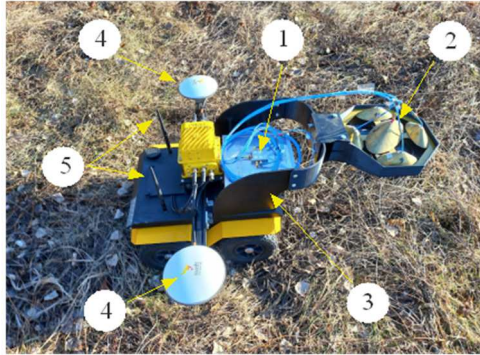


Fig. 3. Main parts of the GPR robot are: 1) GPR hardware unit; 2) antenna system; 3) Jackal robotic platform; 4) GNSS antenna; and 5) WiFi antennas.

but they are all generally silt loam, and the difference should not matter since each field is testing a different sensor. The USA field has never been developed or suffered from war, so it has less clutter than the test fields in Ukraine and Italy, with their urban settings and much longer history of occupation and war.

Taking into account the variety of types of mines used worldwide, we decided to focus on the possibility of detecting two small, LMC AP mines: the USA-made M14 [11] and the Chinese Type 72 [12]. Our reasoning was that if we can remotely detect even a small LMC mine, the same technology can be applied to detect larger plastic-cased mines with greater metal content. By combining this approach (GPR and HSR with MD), we can reliably detect the majority of landmines. We created test fields that measure 1 m by 1 m, containing M14 and Type 72 ultra-realistic simulants (procured from Fenix, U.K.) buried under 2 cm of the local native soil and placed at positions reported in Table I. The buried targets were scanned at least one month after the time of burial to ensure detection of the object and not the disturbed soil. False alarms were evaluated only for the test field for robot #1, with real-time detection and positioning implemented with the GPR. The MD and HSR scanned the positions of objects detected by the GPR system.

#### IV. DESCRIPTION OF THE CAPABILITIES OF THE MULTIPLE SENSORS

##### A. Impulse GPR

The UWB impulse GPR can detect objects that differ in dielectric constant, electrical conductivity, and/or magnetic permeability from the surrounding soil [19], [20], [21], [22]. Such objects include all-plastic or LMC mines.

The GPR (see Fig. 3) is installed on the Jackal robotic platform [16], which is equipped with a GNSS navigation system providing remote control over the robot's movement using a WiFi connection link.

The configuration of the GPR is a 1Tx-4Rx antenna system (Fig. 4) [23]. Short electromagnetic pulses are transmitted into the earth and reflected by buried objects to provide high spatial resolution for the detection of small targets. The spectrum of the sounding signal measured at half of the maximum amplitude spans the frequency band from 0.8 to 1.6 GHz.

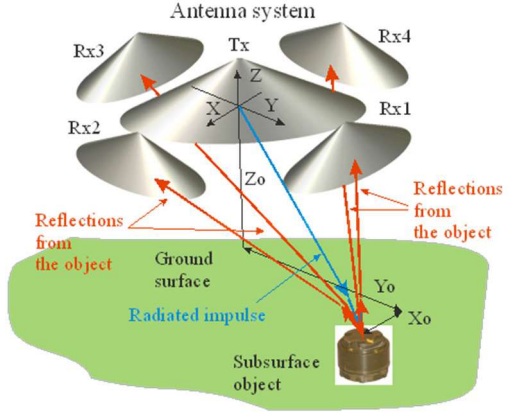


Fig. 4. 1Tx-4Rx antenna system over the ground containing the subsurface object.

This configuration makes it possible to determine the location of a subsurface object using the TOF correlation procedure in real time as the radar is moving [24] without mechanical sweeping or scanning. This positioning has an accuracy of several centimeters (i.e., within the footprint of the target). The detection limit depth for buried objects is approximately 20 cm. With this system, the width of a scanned lane is up to 40 cm, or the same as the width of the robotic platform.

##### B. Metal Detector

The test bed containing the LMC mine targets was searched with a high-performance military grade MD, the CEIA MIL D1 (produced in Italy), mounted on a Jackal robotic platform with the center of the scanning coil mounted 60 cm in front of the metal robot and with a maximum height of 9 cm from the ground. This distance of 60 cm was chosen since it is the minimum distance for which the robot and its metal frame do not interfere with the functioning of the MD. We fixed the MD in a temporary fashion to the robot to check the detectability of these mines. This was not a permanent solution but served well for this test and to derive quantitative information for the final design (see Fig. 5). This solution is easier to implement than the alternative with an MD mounted on a scanning arm [25] because the robotic platform can move along the inspection lane at a higher speed. In our system, the coil has been chosen so that the effective lane width with maximum sensitivity is almost the same as the robot width at 40 cm.

##### C. Holographic Subsurface Radar

The HSR has been developed for obtaining microwave imaging based on variations in the electromagnetic properties of subsurface targets from the surrounding soil [26], [27]. The main electronic components of this type of radar are shown in Fig. 6. The antenna operates at 2 GHz and is produced with a 3-D printer [26]. It generates a continuous wave (CW) monochromatic probing field that can penetrate the soil up to 20 cm [28], depending on the moisture content. The reflected CW signals from the soil surface and the reflective buried object are mixed in the circulator (connector 2) with the transmitted signal (input 1) leaked by the insulator

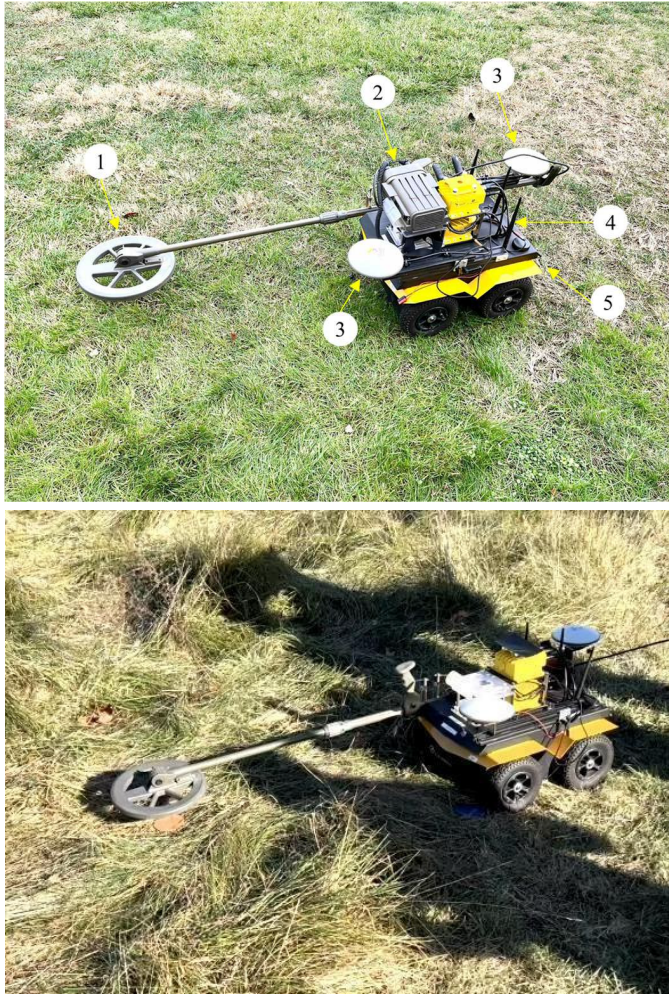


Fig. 5. (Top) CEIA Mil D1 MD mounted on the robotic platform: 1) MD coil, the center of which is at the minimum offset distance of 60 cm from the metal robot frame to avoid any reduction in sensitivity from interference; 2) MD control unit; 3) GPS receiver; 4) WiFi antenna; and 5) Jackal robotic platform. (Bottom) MD system in real field conditions with the coil over the buried Type 72 mine (not visible beneath a vinyl marker).

at Section II. This generates an amplitude/phase modulated signal (output 3). The electronic unit is an ADALM PLUTO module that provides real-time processing for the amplitude and phase information necessary to generate an image in real time. Each pair of values is represented as pixels with color-coded intensity in the grid defined by the electromechanical scanner. The scanner moves the antenna systematically over an investigation area of  $30 \times 24$  cm [26]. It is worth noting that the electronic hardware needed is very simple and has low cost, so it can easily be installed in any scanning system for microwave imaging at close range. Reflections from the robot's metal frame are mitigated by keeping the antenna at least 5 cm from the frame, a distance dictated by the antenna's design with its directivity and specially designed metal shield.

This HSR has a different architecture from other devices intended for commercial use. For example, it differs from the RASCAN type in the signal acquisition mode, in the non-programmable electronics, and in the mechanical acquisition of the samples. Our HSR differs from the HSIR [29]. In our radar, there is a single TX/RX antenna, and the electronic

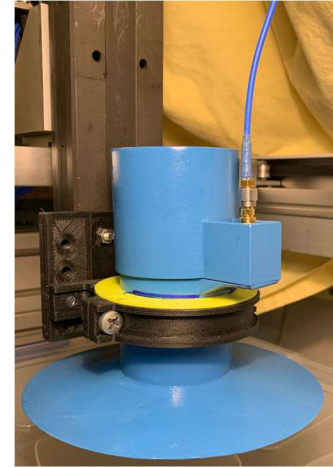


Fig. 6. (Top) 3-D printed 2 GHz antenna with connector to single feed. (Bottom) HSR simplified block scheme.

unit is based on a software-defined radio (SDR) Adalm-Pluto (Analog Devices, USA); this design choice permits a large flexibility in the management of electromagnetic parameters. The reason for these differences is linked to the use case. This device is intended for antipersonnel mine detection in different natural and urban environments; furthermore, due to the presence of surface irregularities and vegetation, it does not work in contact with the ground. SDR-based front-end electronics allows high versatility in the frequency used waveforms and electromagnetic parameters. With regard to the possibility of reconstructing the electromagnetic field at a given distance from the antenna (typically from 5 to 25 cm), according to the theory of holography [30], [31], [32], [33], we found that the raw image obtained in real time is generally sufficient. However, we have experimented with the application of angular spectrum reconstruction and antenna response deconvolution to enhance the image for a more effective interpretation [27].

Fig. 7 lists the main components of the robotic platform carrying the HSR. The bottom of Fig. 7 also shows two pictures that were taken during the scanning of the test field.

## V. EXPERIMENTAL RESULTS

In this section, the experimental results that were obtained sequentially by the GPR, MD, and HSR are reported.

### A. Ground Penetrating Radar

During the period of August to October 2024, we conducted 11 sets of soundings of the test field. We used the collected data to estimate the probability of detection (PD) for the two

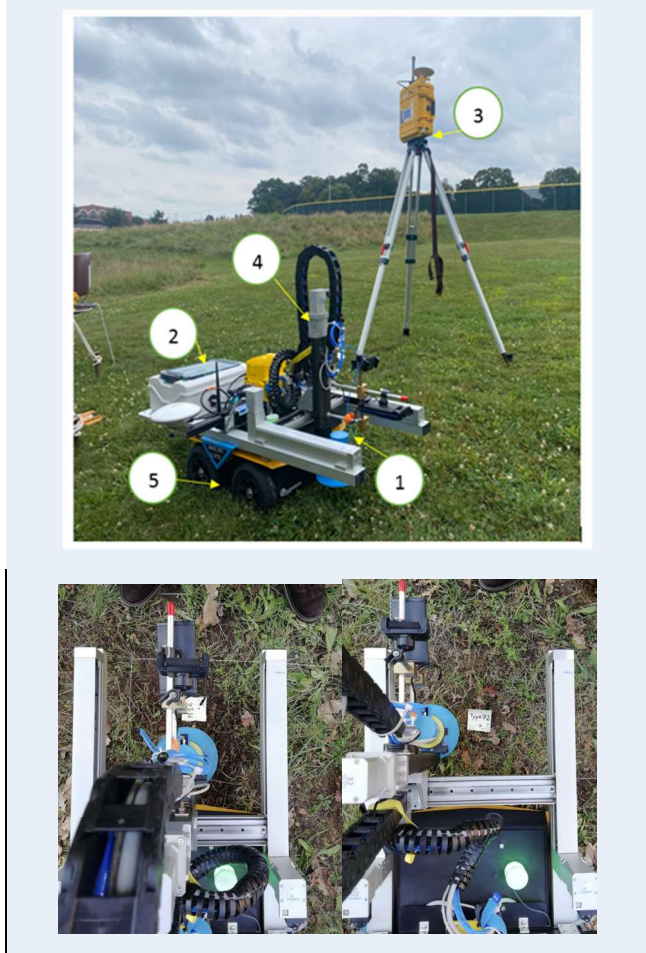


Fig. 7. (Top) Robotic platform with the HSR: 1) HSR sensor; 2) electronic control unit; 3) GPS base station; 4) mechanical scanner; and (5) robot platform. (Bottom) View of the HSR system during the scanning of M14 and Type 72 mines buried in natural soil of the test field in Italy.

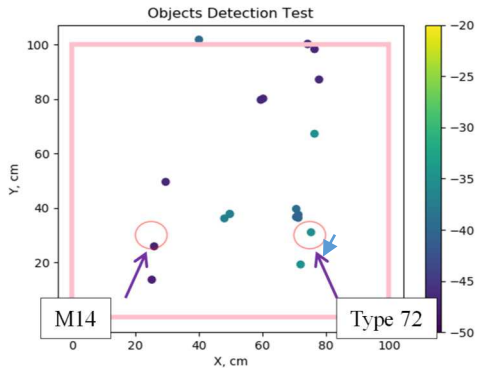


Fig. 8. Points show the positions of detected subsurface objects. The circles correspond to the actual locations of the mine simulants in the test field. The color scale on the right shows the distance (about 35 cm) from the antenna system to the object.

LMC mines in different soil moisture conditions. Examples of typical results of mine detection are shown in Fig. 8.

The object detection algorithm [34] involves calculating two important metrics: the normalized energetic coefficient (SQ) and the correlation coefficient (CC). The SQ is determined by summing the squares of the amplitudes within a specific time window, indicating the presence of a signal. The CC compares

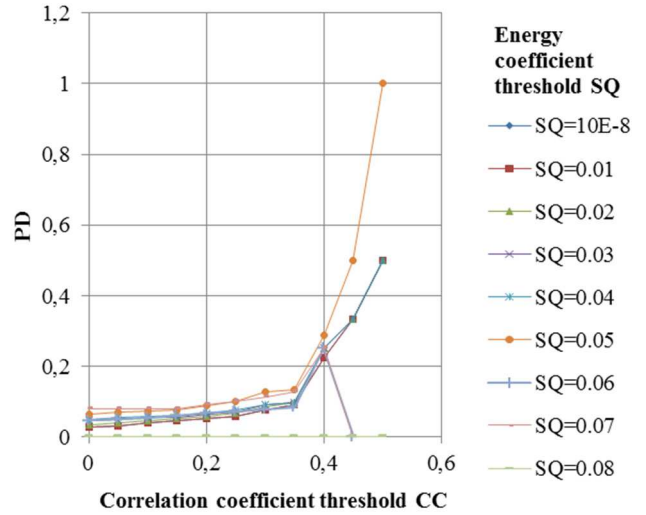


Fig. 9. PD of the Type 72 versus SQ and CC. PD = 1 when CC = 0.5 and SQ = 0.05.

these data to a reflection sample from a metal plate, which is essential for TOF calculations. Both coefficients are critical for determining PD.

We have chosen nine levels of the SQ (from 0 to 0.08) and five levels of the CC (from 0 to 0.5), and checked at which levels combination detection is provided, at which levels it is not provided, and how many true/false detections are in a determined area.

We used the raw data from 11 surveys to calculate the PD as the ratio of the number of correct detections to the total number of detections (e.g., the number of marks shown in Fig. 8) for M14 and Type 72 mines at various thresholds of CC and SQ.

Fig. 9 presents processed data collected on Oct 12, 2024 for the Type 72 mine, assuming the reference signal comes from a reflection from the metal plate.

Usually, the plastic shells of LMC landmines are of small thickness (around 2 mm), and because of this, it does not notably influence GPR detection. Therefore, reflection of electromagnetic waves from the LMC is primarily conditioned by reflection by the boundary between the soil and the explosive. A portion of data on the permittivity of explosives useful to GPR is presented in [35]. As can be seen, the permittivity is mainly in the range between 2.8 and 3.0. The difference between the permittivity of soil and the explosive provides a reflection of the electromagnetic wave and LMC landmine detection. The bigger the difference, the better the detection.

The detection of the plastic-cased LMC mines, and consequently the PD, is influenced by the electromagnetic contrast between the mine casing and the surrounding soil, which strongly depends on the soil moisture content. Therefore, during our experimental session, we recorded data on the moisture content of the soil. To calculate the relative permittivity  $\epsilon$  of the soil, we used the Topp equation [36]

$$\epsilon = 3.03 + 9.3 * \theta + 146 * \theta^2 - 76.7 * \theta^3 \quad (1)$$

where  $\theta$  is the soil moisture content.

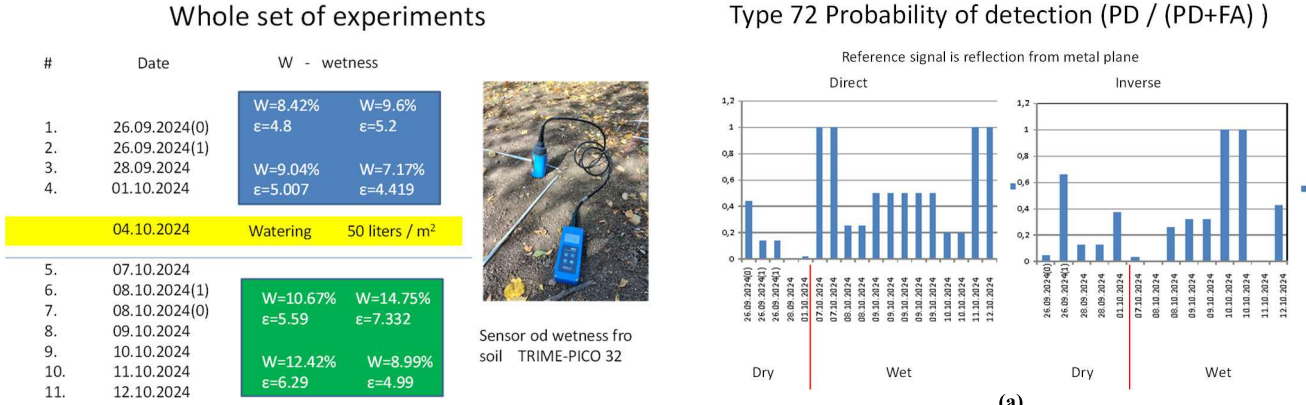


Fig. 10. Soil moisture volume percentage ( $W$ ) and relative permittivity ( $\epsilon$ ) of the soil before and after watering. (Left) there are the experiment numbers and corresponding dates. (Right side) is the soil moisture meter.

We watered the soil for part of the tests because it had become dry after several hot summer months (Fig. 10).

Fig. 11 demonstrates how many detections were made and what PD was registered during the set of experiments in 2024 (a) and (b), and a set of experiments in 2025 (c). There are estimates for the dry soils (on the left part of the Fig. 11(a) and (b), separated by a red vertical line) and wet soil on the right. Dry soil is characterized by relative permittivity in the range from 4.42 to 5.2. For wet soils, it is in the range from 4.99 to 7.33. In Fig. 11(c), there is no “dry soil” section. Because of rainy weather, the soil moisture content was within 15.8%–21.2%, which, according to the Topp equation (1), means a permittivity in the range from 8.7 to 12.5.

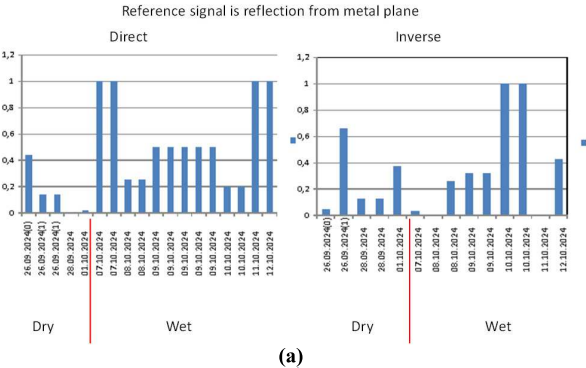
The CC is “direct” if the reference signal is a reflection from the metal plate and “inverse” if the signal of the opposite sign is used as a reference signal. All data are included. The dates of experiments (in format DD.MM.YYYY) are on the horizontal axis.

Fig. 11(a) demonstrates an increasing number of higher PDs of Type 72 after watering. During the four days before watering, we had only one PD = 0.66. After watering, over seven days of experiments, we obtained four PD = 1 and, after five days, PD = 0.5. This indicates that after watering the soil, the Type 72 became much more readily detectable. In this case, correlation with the direct signal is better.

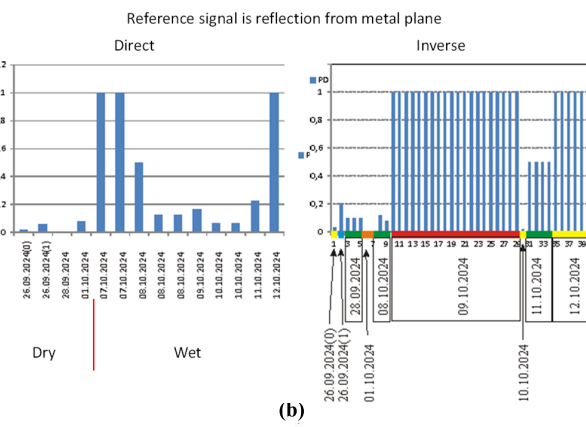
Fig. 11(b) and (c) are about the detection of M14. Practically all descriptions of the landmine M14, for example, [37], state that there is only a small “steel firing pin” in the mine. However, in the same and other sources, for example [38] or [39], authors indicate that “The M14 AP mine has been modified by gluing a metal washer to the bottom of the mine. The modification was directed to improve the detectability of the mine. Unmodified mines are not authorized for use by US forces.” So, there is a metal washer glued to the M14. Therefore, in the first series of experiments conducted in 2024, we used a surrogate of the M14 mine with a metal washer. Statistics on its detection are shown in Fig. 11(b).

However, production and application of the M14 is not only under the control of the US. Since it is possible to remove the metal washer, the landmine can truly become a mine of

### Type 72 Probability of detection (PD / (PD+FA) )



M14 Probability of detection (PD / (PD+FA) )



M14 without metal washer  
Probability of detection (PD / (PD+FA) )

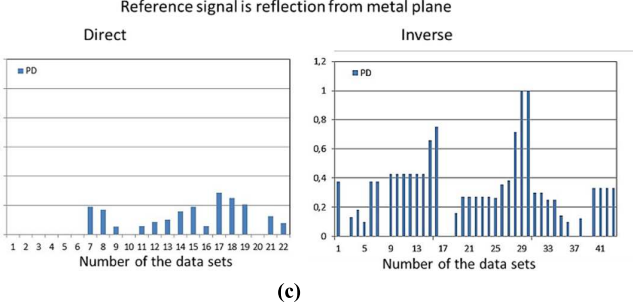


Fig. 11. (a) Maximal value of PD and numbers of PD for Type 72, (b) M14 with a metal washer in dry and wet soil conditions, and (c) LMC M14 without a metal washer.

“minimal metal content.” Therefore, we decided to add the results of a series of experiments with a surrogate of the M14 mine from which the metal washer was removed. The results of these measurements are added to the materials of this article in Fig. 11(c).

Fig. 11(b) shows that for dry soil, the largest PD of M14 is very low (0.2 or less), independent of a direct or inverse reference signal. The situation is completely reversed for wet soil. After watering, the small LMC M14 mine also became much more detectable. We can see that radar data of 09, 11, and 12 October gave us PD = 1 for 27 trials at a wide range of CC and SQ from 0.06 to 0.08.

TABLE I

TARGET POSITIONS ( $X$ ,  $Y$ ) WITH REFERENCE SYSTEM SHOWN IN FIG. 2

Target	M14	Type 72
Mapped Position X [cm], Y [cm]	25 cm, 30 cm	75 cm, 30 cm

TABLE II

LMC DETECTION CHARACTERISTICS WITH GPR

Target	Soil			
	Wet		Dry	
	PD <sub>max</sub>	N*	PD <sub>max</sub> **	N
M14	1	30	0.2	1
Type 72	1	6	0.64	1

\* $N = 30$  means that M14 was detected 30 times with  $PD_{max}=1$ \*\* $PD_{max} = 0.2$  means that even at the optimal SQ and CC only 1 detection from 5 corresponds to M14

As shown in Fig. 11(c), the M14 mine without a metal washer, when placed in wet soil, is still “detectable.” This detection is particularly effective if the software designed to detect the LMC mine is configured for plastic mines, using the “inverse” signal as a reference. However, there is a key difference: unlike the detection of the M14 with a metal washer depicted in Fig. 11(b), which consistently produces a detection probability close to 1 regardless of the detection parameter settings (such as CC and SQ), the probability of detecting the M14 without a metal washer is generally lower. It typically exceeds 0.3 and can occasionally reach a probability of 1.

To summarize the results of experiments with the GPR, we present statistics of detections as the best PD in *wet* soil—and the number of these best detections/the best PD in *dry* soil—and the number of these best detections N obtained at 11 acquisitions. The probability of GPR detection if the deviation of the detected position from the center of mine is less than 5 cm is shown for Robot #1 in Table II.

There is an electromagnetic explanation for this phenomenon: 1) Watering increased the dielectric contrast between the soil and mine casing. This led to an increase in the reflection coefficient, and therefore, an increase in the amplitudes of the reflected waves and 2) the reflection coefficient of electromagnetic waves from the metal plate has a negative sign. This signifies the opposite polarity of the reflected electromagnetic wave. If we use a direct signal as a reference for correlation, the resulting CC becomes negative, and our algorithm filters it out. If the soil is watered, the reflected wave keeps its polarity as the permittivity of the upper layer of ground at the boundary between the mine and soil is larger than the permittivity of M14. Therefore, to get a higher CC, we must use an inverted reference signal. Both the elevated contrast between plastic and soil due to watering and considering the sign of CC help to achieve a much higher PD at a wide range of coefficients CC and large SQ.

TABLE III

CEIA MILD1 MD MINE DETECTION RESULTS

Output signal processing for pinpointing	2 tones /digital output on/off
Coil diameter	28 cm
Weight of coil + boom	1.6 kg
Detection lane maximum width (Type 72, M14, PMN-1, PMN-4)	14 cm, 18 cm, 36 cm, 62 cm
Detection maximum height (Type 72, M14, PMN-1, PMN-4)	11 cm, 9 cm, 19 cm, 25 cm
Metal cart distance required for negligible interference (Type 72, M14)	60 cm, 60 cm

For practical mine detection, before the start of scanning, we can measure soil moisture. If it is 12% or higher (Fig. 7), we can choose the reverse signal as a reference and expect a high PD of small plastic mines. Even if the MD does not provide a response at that location, we can confidently interpret the reflections as representing a small plastic target or possible LMC mine.

If a CC is high for the direct reference signal, it indicates that the buried target is metal. Detection of such a target by the MD would confirm the UWB GPR detection.

### B. Metal Detector

According to the MD manual, detection requires sweeping in *a*-direction perpendicular to the boom (see the green colored boom in Fig. 5). As mounted in the figure, lateral sweeping of the coil is required to detect metal objects. In principle, the coil could be rotated 90° and fixed, thereby allowing detection with forward movement alone. Note that this would require a secondary sweep in the perpendicular direction after detection if one wanted to localize the mine position in the lateral direction. In our case, we have used the MD to confirm the (already localized) mine detections from the GPR, but we have not independently localized them in both directions with the MD. In Table III, we report quantitative data for the detection of the M14 and Type 72 LMC landmines in the test bed.

The ground at the test field was a silty clay soil with grass under moderately humid conditions. We detected both the M14 and Type 72 buried mines, each of which was buried at a depth of 2 cm.

The MD confirmed the detections of GPR when the coil was about 7 cm from ground, while at greater heights it did not.



Fig. 12. Photograph of the  $1 \times 1 \text{ m}^2$  test field with the two target positions (bottom left) M14 and (bottom right) Type 72. The area has an irregular surface and is partially covered by leaves that fall in the season.

We detected no false alarms in the search of the area since the soil is natural and not contaminated with metal clutter or other debris. Note that we also tested (in a nearby bed) the Russian-made PMN-1 and PMN-4 AP mines that contain significant metal, and these were readily detected at coil heights up to 25 cm at lateral offsets up to 31 cm effective (lane width 62 cm) for the PMN-4.

### C. Holographic Subsurface Radar

The test field at UNIFI followed the same design shown in Fig. 2. The photograph of the area with the tagged positions of the two targets is shown in Fig. 12.

The most difficult targets were identified as round-shaped features in the microwave images, obtained in the Italian test field, with a soil water content of 30%. The HSR frequency was selected to be 2.05 GHz. The irregular soil surface is shown by the LiDAR images in Figs. 13 and 14.

The investigation of the HSR imaging at various heights of the antenna from the ground is important because the system must operate with different soil roughness and vegetation conditions. Scanning with the antenna as close as 4 cm to the ground (e.g., Figs. 13 and 14) is an advantage because of the strong coupling with the soil. A larger antenna height reduces the electromagnetic coupling with the ground and lowers the phase variation sensitivity. Also, the higher the antenna position, the more likely the system is to experience reflections of the CW transmitted field from surrounding objects on the surface, and the system will also operate with a lower field power density at the surface. For comparison, a set of acquisitions were made on a different day at heights of 4, 7, 10, and 13 cm (see Fig. 15). For the Type 72 mine, the increase of the height to 13 cm did not significantly change the imaging capability to describe a round shaped object, though the best image is at a height of 7 cm. For the M14 that was located closer to the robot metal cart (left side of the image), the best

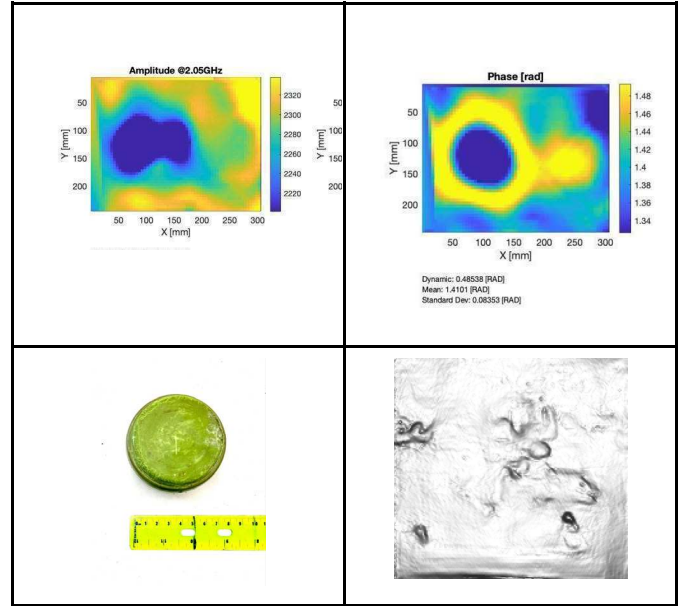


Fig. 13. (Top) Type 72 landmine. (Left) HSR amplitude and (right) phase images of the Type 72 mine. (Bottom) Photograph of the Type 72 landmine simulant (Left) and LiDAR image of the area where the landmine simulant was buried. At the bottom of the LiDAR image, a ruler appears horizontally, with a length 30 cm. The quasi-circular contour in the phase image (top right) shows the mine location with a diameter of about 9 cm. Inside the circle the phase variation is minimal and appears as a uniform color.

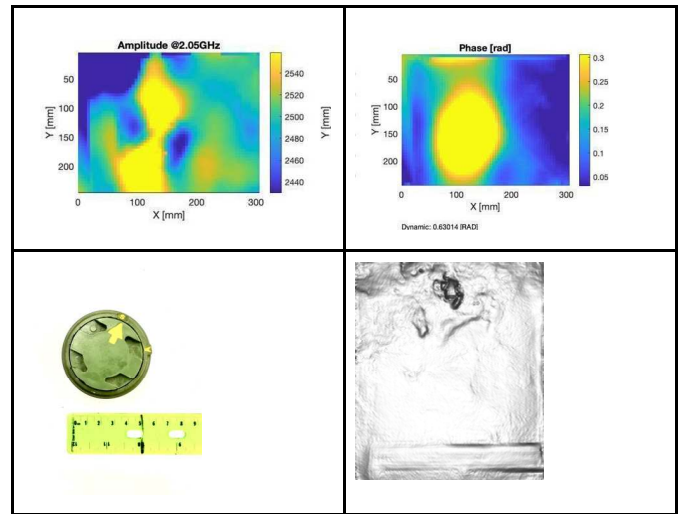


Fig. 14. (Top) M14 landmine. (Left) Amplitude and (right) phase plots of the M14 mine. The amplitude image reproduces the distinctive shape of the plastic case of this mine. The bilateral structure in the amplitude image corresponds to the symmetry axis of the structure on the top of the mine. The phase image shows an elliptical shape with axis lengths  $10 \times 12 \text{ cm}$ . (Bottom) Photograph of the M14 landmine simulant with similar bilateral orientation at the HSR amplitude image (Left) and LiDAR image of the area where the landmine simulant was buried. On the bottom of the LiDAR image appears horizontally a ruler with length 30 cm.

isolated target can be discriminated at 7 cm but with a stronger influence of soil surface and possibly a reflection from the cart. At 10 and 13 cm heights, the image discrimination is worse than at 4 and 7 cm.

This second set of images at different heights was acquired on a different day with a soil water content of 40%.

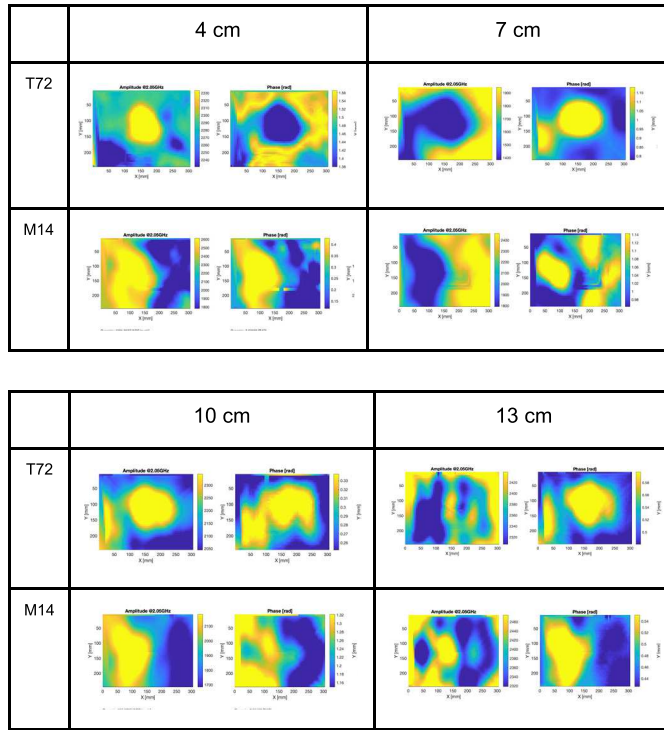


Fig. 15. HSR scan of Type 72 and M14 landmines at the height indicated on the top rows of the table.

TABLE IV  
MINE DETECTION RESULTS

Target	M14	Type 72
Robot #1 GPR	Y	Y
Robot #2 MD	U	U
Robot #3 HSR	D	D
Overall Detection/Discrimination by System	Y	Y

#### Legend:

Y = detected

N = not detected

U = detected, but target uncertain

D = detected and discriminated

#### D. Results From Combined Sensor Data

In Table IV, we present the overall detection results from the various sensors.

This table presents a grid of detectability of the two LMC mine types using the combination of the three different sensors. Note that the MD confirmed the initial detections of the GPR when the MD coil was about 7 cm from the ground, while at higher distances, it did not detect them. In addition, the MD cannot inherently discriminate mines from clutter, so the detection has been evaluated as uncertain. The initial detections with the GPR were possible at a height of about

33 cm (see Fig. 2). The HSR performed the imaging at about 4 cm from the ground, but we also obtained very good images at higher distances (up to 13 cm) and in different soil conditions. At higher distances, the effect of soil surface response becomes more relevant, and possible reflections from the metal Jackal can be superimposed on the weaker reflections from LMC landmines.

#### VI. DISCUSSION AND CONCLUSION

LMC AP landmines Type 72 and M14 can be detected according to standard operating procedures with a manual handheld MD when swept very close to the ground (less than 9 cm). Unfortunately, this operation is not applicable for all soil conditions and is risky for the operator.

The wideband GPR mounted on robot #1 can detect the two targets at a level of precision within their diameters. The greatest PD for both M14 and Type 72 is unity, but only after watering the soil to increase the dielectric contrast with the plastic casings of the mines. The GPR must be initially calibrated on a metal reflector to set the proper value of the detection threshold parameter.

The MD mounted on robot #2 can detect the targets and determine precise positioning along the lane only when the MD is very close to the ground (less than 9 cm) and when the electronic unit is set to the maximum sensitivity. However, in conditions other than the very clean USA test bed, the latter condition will also increase the number of false alarms.

The HSR mounted on robot #3 produced high-quality images for the Type 72 that can be used to discriminate a round-shaped target in the correct position and with a diameter compatible with the target. The images remain quite similar up to a height of 13 cm. We found that clutter in the Italy test bed is more evident at a greater height. The electromagnetic image contrast was highest at a soil moisture content of 30%–40% by weight. The scanning time for data acquisition is on the order of 2 min, so this information can be acquired only on selected positions dictated by the previous data acquisitions with the GPR and MD.

According to the results in this work, the multisensor approach provides a more robust and versatile detection of LMC landmines with respect to the standard operating procedure using handheld MD instruments or direct probing. The three different sensors mounted on robotic platforms operate remotely, reducing risk for operators, and the GPR and HSR sensors can operate at a distance from the ground greater than 10 cm. This is an acceptable condition for rough soil surfaces and areas with vegetation.

When the MD is completely integrated into the system in a more advanced stage of development, we will use the MD detections to localize objects identified by the impulse GPR.

#### ACKNOWLEDGMENT

The authors wish to acknowledge the support of the NATO SPS MYP PROJECT G-7563 “Innovative Sensor Integration for Remote Landmine Detection,” <https://www.natospsdeminingrobots.com/>

## REFERENCES

- [1] (2024). *LANDMINE MONITOR 2024*. [Online]. Available: <https://backend.icblcmc.org/assets/reports/Landmine-Monitors/LMM2024/Downloads/Landmine-Monitor-2024-Final-Web.pdf>
- [2] E. Vivoli, M. Bertini, and L. Capineri, "Deep learning-based real-time detection of surface landmines using optical imaging," *Remote Sens.*, vol. 16, no. 4, p. 677, Feb. 2024, doi: [10.3390/rs16040677](https://doi.org/10.3390/rs16040677).
- [3] L. Capineri et al., "Multi-sensor cooperative robots for shallow buried explosive threat detection: Radar sensors and optical sensors integrated by system software," in *Proc. 13th Int. Workshop Adv. Ground Penetrating Radar (IWAGPR)*, Greece, Jul. 2025, pp. 1–5.
- [4] IEEE Standard for Ultrawideband Radar Definitions, Standard 1672-2006, May 2007, pp. 1–19, doi: [10.1109/IEESTD.2007.359972](https://doi.org/10.1109/IEESTD.2007.359972).
- [5] D. J. Daniels, *Surface Penetrating Radar*. London, U.K.: IEE, 1996.
- [6] E. Vivoli, L. Capineri, and M. Bertini, "HoloMine: A synthetic dataset for buried landmines recognition using microwave holographic imaging," *IEEE J. Sel. Topics Appl. Earth Observ. Remote Sens.*, vol. 18, pp. 9883–9892, 2025, doi: [10.1109/JSTARS.2025.3555442](https://doi.org/10.1109/JSTARS.2025.3555442).
- [7] S. Ivashov, L. Capineri, and T. Bechtel, "Holographic subsurface radar technology and applications," in *Ultrawideband Radar: Applications and Design*, J. D. Taylor, Ed., Boca Raton, FL, USA: Taylor & Francis, 2012, pp. 421–444.
- [8] L. Capineri et al., "RASCAN holographic radar for detecting and characterizing dinosaur tracks," in *Proc. 7th Int. Workshop Adv. Ground Penetrating Radar*, Jul. 2013, pp. 1–6, doi: [10.1109/IWAGPR.2013.6601553](https://doi.org/10.1109/IWAGPR.2013.6601553).
- [9] M. García-Fernández, G. Álvarez-Narciandi, Y. Álvarez López, and F. Las-Heras Andrés, "Improvements in GPR-SAR imaging focusing and detection capabilities of UAV-mounted GPR systems," *ISPRS J. Photogramm. Remote Sens.*, vol. 189, pp. 128–142, Jul. 2022, doi: [10.1016/j.isprsjprs.2022.04.014](https://doi.org/10.1016/j.isprsjprs.2022.04.014).
- [10] M. Schartel, R. Burr, R. Bähnemann, W. Mayer, and C. Waldschmidt, "An experimental study on airborne landmine detection using a circular synthetic aperture radar," 2020, *arXiv:2005.02600*.
- [11] M. G. Fernández et al., "Synthetic aperture radar imaging system for landmine detection using a ground penetrating radar on board a unmanned aerial vehicle," *IEEE Access*, vol. 6, pp. 45100–45112, 2018, doi: [10.1109/ACCESS.2018.2863572](https://doi.org/10.1109/ACCESS.2018.2863572).
- [12] D. Šipoš and D. Gleich, "A lightweight and low-power UAV-borne ground penetrating radar design for landmine detection," *Sensors*, vol. 20, no. 8, p. 2234, Apr. 2020, doi: [10.3390/s20082234](https://doi.org/10.3390/s20082234).
- [13] *Study on Evaluating Airborne GPR's Potential for UXO and Landmine Detection in a Controlled Environment*. Accessed: Oct. 18, 2025. [Online]. Available: <http://www.sphengineering.com> and <https://www.sphengineering.com/news/study-on-evaluating-airborne-gprs-potential-for-uxo-and-landmine-detection-in-a-controlled-environment>
- [14] J. Colorado et al., "An integrated aerial system for landmine detection: SDR-based ground penetrating radar onboard an autonomous drone," *Adv. Robot.*, vol. 31, no. 15, pp. 791–808, Aug. 2017, doi: [10.1080/01691864.2017.1351393](https://doi.org/10.1080/01691864.2017.1351393).
- [15] C. Noviello et al., "An overview on down-looking UAV-based GPR systems," *Remote Sens.*, vol. 14, no. 14, p. 3245, Jul. 2022, doi: [10.3390/rs14143245](https://doi.org/10.3390/rs14143245).
- [16] Clearpath Robotics. (2015). *Jackal UGV-Small Weatherproof Robot-Clearpath*. [Online]. Available: <https://clearpathrobotics.com/jackal-small-unmanned-ground-vehicle/>
- [17] Cat-uxo.com. (2024). *CAT-UXO-M14 Landmine*. Accessed: Dec. 20, 2024. [Online]. Available: <https://cat-uxo.com/explosive-hazards/landmines/m14-landmine>
- [18] Cat-uxo.com. (2024). *CAT-UXO-Type 72 Ap Landmine*. Accessed: Dec. 20, 2024. [Online]. Available: <https://cat-uxo.com/explosive-hazards/landmines/type-72-ap-landmine>
- [19] J. D. Taylor, *Ultrawideband Radar*. Boca Raton, FL, USA: CRC Press, 2016.
- [20] H. M. Jol, *Ground Penetrating Radar Theory and Applications*. Burlington, NJ, USA: Elsevier, 2009.
- [21] R. Persico, *Introduction to Ground Penetrating Radar*. Hoboken, NJ, USA: Wiley, 2014.
- [22] K. Furuta and J. Ishikawa, *Anti-Personnel Landmine Detection for Humanitarian Demining*. Cham, Switzerland: Springer, 2009.
- [23] G. Pochanin et al., "Design and simulation of a 'single transmitter-four receiver' impulse GPR for detection of buried landmines," in *Proc. 9th Int. Workshop Adv. Ground Penetrating Radar (IWAGPR)*, Jun. 2017, pp. 1–5. [Online]. Available: <http://ieeexplore.ieee.org/stamp/stamp.jsp?tp=&arnumber=7996112>
- [24] G. P. Pochanin et al., "Measurement of coordinates for a cylindrical target using times of flight from a 1-transmitter and 4-receiver UWB antenna system," *IEEE Trans. Geosci. Remote Sens.*, vol. 58, no. 2, pp. 1363–1372, Feb. 2020, doi: [10.1109/TGRS.2019.2946064](https://doi.org/10.1109/TGRS.2019.2946064).
- [25] S. Dogru and L. Marques, "Estimating depth of buried metallic objects," in *Proc. IEEE Sensors*, New Delhi, India, Oct. 2018, pp. 1–4, doi: [10.1109/ICSENS.2018.8589731](https://doi.org/10.1109/ICSENS.2018.8589731).
- [26] L. Bossi, P. Falorni, S. Priori, R. Olmi, and L. Capineri, "Numerical design and experimental validation of a plastic 3D-printed waveguide antenna for shallow object microwave imaging," *Sens. Imag.*, vol. 22, no. 1, pp. 1–24, May 2021, doi: [10.1007/s11220-021-00344-4](https://doi.org/10.1007/s11220-021-00344-4).
- [27] L. Bossi, P. Falorni, and L. Capineri, "Versatile electronics for microwave holographic RADAR based on software defined radio technology," *Electronics*, vol. 11, no. 18, p. 2883, Sep. 2022, doi: [10.3390/electronics11182883](https://doi.org/10.3390/electronics11182883).
- [28] L. Bossi, P. Falorni, F. Crawford, T. Bechtel, V. Plakhtii, and L. Capineri, "Water-filled testbed modeling, design, and fabrication for performance validation of a holographic subsurface RADAR antenna," in *Proc. 11th Int. Workshop Adv. Ground Penetrating Radar (IWAGPR)*, Valletta, Malta, Dec. 2021, pp. 1–4, doi: [10.1109/IWAGPR50767.2021.9843147](https://doi.org/10.1109/IWAGPR50767.2021.9843147).
- [29] H. Zhihua et al., "A holographic subsurface imaging radar with high plane resolution: Principle and application," *J. Phys., Conf. Ser.*, vol. 2887, no. 1, Nov. 2024, Art. no. 012020, doi: [10.1088/1742-6596/2887/1/012020](https://doi.org/10.1088/1742-6596/2887/1/012020).
- [30] D. Sheen, D. McMakin, and T. Hall, "Near-field three-dimensional radar imaging techniques and applications," *Appl. Opt.*, vol. 49, no. 19, p. E83, Jun. 2010, doi: [10.1364/ao.49.0000e83](https://doi.org/10.1364/ao.49.0000e83).
- [31] U. Schnars and W. P. O. Jüptner, "Digital recording and numerical reconstruction of holograms," *Meas. Sci. Technol.*, vol. 13, no. 9, Aug. 2002.
- [32] G. T. Nehmetallah, R. Aylo, and L. Williams, *Analog and Digital Holography With MATLAB*. SPIE, 2015.
- [33] R. Aylo, G. T. Nehmetallah, and L. Williams, *Analog and Digital Holography With MATLAB*. Bellingham, WA, USA: SPIE, Aug. 2015. [Online]. Available: <https://spiedigitallibrary.org/ebooks/PM/Analog-and-Digital-Holography-with-MATLAB/eISBN-9781628416596/10.1117/3.2190844>
- [34] (2025). *Spiedigitallibrary.Org*. Accessed: Sep. 11, 2025. [Online]. Available: <http://opticalengineering.spiedigitallibrary.org/article.aspx?doi=10.1117/1.600706>
- [35] D. J. Daniels, "A review of GPR for landmine detection," *Sens. Imag., Int. J.*, vol. 7, no. 3, pp. 90–123, Sep. 2006, doi: [10.1007/s11220-006-0024-5](https://doi.org/10.1007/s11220-006-0024-5).
- [36] G. C. Topp, J. L. Davis, and A. P. Annan, "Electromagnetic determination of soil water content: Measurements in coaxial transmission lines," *Water Resour. Res.*, vol. 16, no. 3, pp. 574–582, Jun. 1980, doi: [10.1029/wr016i003p00574](https://doi.org/10.1029/wr016i003p00574).
- [37] Army.mil. (2025). *ODIN-OE Data Integration Network*. [Online]. Available: <https://odin.tradoc.army.mil/WEG/Asset/6c49b8ebae058cdce69720c833452859f>
- [38] J. Pike. (2025). *FM 20-32 CHAPTER 5*. GlobalSecurity.org. [Online]. Available: [https://www.globalsecurity.org/military/library/policy/army/fm-20-32/chap5.html?utm\\_source=chatgpt.com#google\\_vignette](https://www.globalsecurity.org/military/library/policy/army/fm-20-32/chap5.html?utm_source=chatgpt.com#google_vignette)
- [39] Olly. (Dec. 2020). *M14 'Toe Popper' Anti-Personal Mine-MACV-SOG*. Modernforces.co.uk. [Online]. Available: [https://modernforces.co.uk/2020/12/04/m14-anti-personal-mine/?utm\\_source=chatgpt.com](https://modernforces.co.uk/2020/12/04/m14-anti-personal-mine/?utm_source=chatgpt.com)



**Lorenzo Capineri** (Senior Member, IEEE) is a Full Professor in electronics. He has worked on several research projects in collaboration with National (Gilardoni spa) and International Industries (National Semiconductors, Texas Instruments, Marvell, Thales Alenia Space Italia), and Research Institutions: Italian Research Council (CNR), Italian Space Agency (ASI) and European Space Agency (ESA), AEA Technology and UKAEA (England), European Commission Joint Research Centre (Ispra) and NATO (Brussels, Belgium). He is co-author of seven Italian patents and co-author of five book chapters and about 300 peer-reviewed scientific and technical papers. His current research activities are in the design of ultrasonic guided wave devices, buried objects detection with ground penetrating radar, and holographic radar.

Mr. Capineri is the Vice-President of IEEE Italy Sensors Chapter, Co-Chair of IWAGPR2015 conference, Member of Scientific and Technical committee of IUS-IEEE, GPR, PIERS, URSI-GASS, and IWAGPR conferences, and Fellow of Electromagnetic Academy and British Institute of Nondestructive Testing.



**Gennadiy P. Pochanin** (Senior Member, IEEE) was born in Kharkiv, Ukraine, in 1961. He received the M.Sc. and Ph.D. degrees in radiophysics and electronics from Kharkiv State University, Kharkiv, in 1983 and 2003, respectively.

Since 1985, he has been a Scientist with the O.Ya.Usikov Institute for Radiophysics and Electronics of the National Academy of Sciences of Ukraine, Kharkiv, where he is currently a Chief of the Radiophysical Introspection Department. He has co-authored seven books, more than 70 articles, and more than ten inventions. His research interests include transient wave phenomena, radiation and reception of ultrawideband short pulses of electromagnetic waves, ultrawideband antennas, ultrawideband radars, and ground-penetrating radars.

Dr. Pochanin is a Winner of the State Prize of Ukraine in the area of Science and Technology 2016. He received the Senior Researcher Academic Status in 2005.



**Tetiana Ogurtsova** was born in Ukraine, in 1967. She received the degree in applied mathematics from the Faculty of Mechanics and Mathematics, Kharkiv State University, Kharkiv, Ukraine, in 1989. She is currently pursuing the degree in physical and mathematical sciences.

Since then, she has been employed at the O.Ya. Usikov Institute for Radiophysics and Electronics of the National Academy of Sciences of Ukraine, Kharkiv, where she currently serves as a Senior Researcher. Her work focuses on the theoretical and experimental study of ultrawideband receiving antennas, as well as the development of algorithms and software for data processing. She has co-authored more than 30 scientific publications.



**Vadym P. Ruban** was born in Ukraine, in 1979. He received the Dipl.-Ing. degree in radio-physics engineering and the Ph.D. degree in physics of instruments, elements and systems from V.N. Karazin Kharkiv National University, Kharkiv, Ukraine, in 2002 and 2021, respectively.

Since 2002, he has been a Scientist with O.Ya. Usikov Institute for Radiophysics and Electronics of the National Academy of Science of Ukraine, Kharkiv. Currently, he is a Senior Researcher of the Radiophysical Introspection Department. He has co-authored three books, more than 15 articles, and two inventions. His research interests include ground-penetrating radar designing, receiving, and processing of the impulse UWB signals.



**Timothy D. Bechtel** (Member, IEEE) received the B.Sc. degree in geology from Haverford College, Haverford, PA, USA, in 1982, the M.Sc. degree in geology from Brown University, Providence, RI, USA, in 1984, and the Ph.D. degree in geophysics from Brown University, in 1989.

He worked with the Geologic and Environmental Consulting from 1987 through the present at Kurz Associates, Bridgewater, MA, USA, TETHYS Consulting, Harrisburg, PA, USA, Enviroscan, Lancaster, PA, and RETTEW Associates, Lancaster. He returned to academia in 2001, teaching with the Department of Earth and Environmental Science, University of Pennsylvania, Philadelphia, PA, and the Department of Earth and Environment, Franklin and Marshall College, Lancaster. He teaches courses in geophysics, hydrogeology, environmental science, engineering geology, and geocomputation. His current research is on novel sensors for humanitarian demining, karst hydrogeology, and remote sensing for the detection of faults and fractures.

Dr. Bechtel is a Fellow of the Geological Society of America and winner of the Geological Society of America's Public Service Award in 2021.



**Luca Bossi** was born in Prato, Tuscany, Italy, in 1973. He received the master's degree in electronic engineering and the Ph.D. degree in information engineering from the University of Florence, Florence, Italy, in 2018 and 2022, respectively.

He is currently a Post-Doctoral Researcher and a Lower Secondary School Teacher. He deals with microwave RADAR sensors that penetrate the ground. He works in an international research group for the development of new technologies for demining for humanitarian purposes. Since 1996, he has

been working as an Entrepreneur in the retail sector. He is the author/co-author of over 6 articles in journals and 19 conference proceedings. His main interests are in the field of teaching, microwave RADAR, electronics applied to humanitarian issues and Industry 5.0.



**Pierluigi Falorni** was born in Florence, Tuscany, Italy, in 1966. He received the master's degree in informatic engineering and the Ph.D. degree in non destructive testings from Università degli Studi di Firenze, Firenze, Italy, in 1999 and 2005, respectively.

He works as a professional in the field of management of software development projects. He collaborates with the University of Florence, Florence, Italy, as a Freelance Researcher specialized in signal processing algorithms, mainly for landmines detection from radar data.



**Fronefield Crawford** was born in Bryn Mawr, PA, USA, in 1972. He received the B.A. degree in astrophysics from Williams College, Williamstown, MA, USA, in 1994, and the Ph.D. degree in physics from MIT, Cambridge, MA, in 2000.

He teaches courses in physics and astronomy at the Franklin and Marshall College, Lancaster, PA, where he is currently a Professor with Astronomy and the Director of Grundy Observatory, Lancaster. He was previously employed as a Senior Systems Engineer with Lockheed Martin, King of Prussia, PA, where he worked on remote sensing systems. His research interests include the study of radio pulsars using large radio telescopes, the search for low-frequency gravitational waves using pulsars as detectors, and the detection and identification of landmines using remote sensing methods.